

# Interactive Intra-operative 3D Ultrasound Reconstruction and Visualization

David G. Gobbi<sup>1,2</sup> and Terry M. Peters<sup>1,2</sup>

<sup>1</sup> Imaging Research Laboratories,  
John P. Robarts Research Institute, University of Western Ontario,  
London ON N6A 5K8, Canada

dgobbi@imaging.robarts.ca, tpeters@imaging.robarts.ca  
<http://www.imaging.robarts.ca/Faculty/peters.html>

<sup>2</sup> Department of Medical Biophysics, University of Western Ontario,  
London ON N6A 5C1, Canada

**Abstract.** The most attractive feature of 2D B-mode ultrasound for intra-operative use is that it is both a real time and a highly interactive modality. Most 3D freehand reconstruction methods, however, are not fully interactive because they do not allow the display of any part of the 3D ultrasound image until all data collection and reconstruction is finished. We describe a technique whereby the 3D reconstruction occurs in real-time as the data is acquired, and where the operator can view the progress of the reconstruction on three orthogonal slice views through the ultrasound volume. Capture of the ultrasound data can be immediately followed by a straightforward, interactive nonlinear registration of a pre-operative MRI volume to match the intra-operative ultrasound. We demonstrate the our system on a deformable, multi-modal PVA-cryogel phantom and during a clinical surgery.

## 1 Introduction

The intra-operative use of 3D ultrasound during neurosurgical procedures is recent and still very rare. While there are significant advantages to using 3D ultrasound over 2D ultrasound, many technical hurdles remain with respect to optimization of the instrumentation and software. A significant amount of development in this area has been performed by SINTEF in Norway [1,2], leading to a commercial product for neuronavigation with 3D ultrasound. The two specific developments in this field that we are investigating are real-time reconstruction of the 3D ultrasound volumes and the use of multi-modal nonlinear registration to warp pre-operative MR images to match intra-operative ultrasound.

The non-linear registration of MRI to ultrasound is of particular interest because it allows the pre-operative MRI images (along with any contrast enhancement or functional information) to be used for accurate surgical guidance, even in the presence of the significant degree of brain shift [3,4] that is common in most craniotomy procedures.

Our primary focus in this work is to demonstrate how real-time 3D ultrasound reconstruction can be performed on standard computer hardware, and

furthermore how the reconstruction can be integrated into a 3D visualization package to allow visualization of arbitrary slices through the 3D image while data collection is taking place.

## 2 Materials and Methods

Our software platform uses VTK (<http://www.kitware.com/vtk.html>) [5] for 3D rendering and a high-level application framework written in python for the user interface (<http://www.atamai.com>). We have contributed most of the computational C++ code that we developed for this application to the VTK library, including our code for performing nonlinear transformations on images [6].

For image acquisition, we use an Aloka SSD-1700 ultrasound scanner with a 5.0 MHz curved-array neuro ultrasound probe (Aloka Co., Ltd., Tokyo, Japan). The probe is fitted with a set of infrared LEDs that are tracked by a POLARIS optical measurement system (Northern Digital Inc., <http://www.ndigital.com>).

The 3D image reconstruction and visualization is performed using a 2 CPU 933 MHz Pentium III workstation in real time as the the B-mode ultrasound video and POLARIS tracking measurements are acquired. The C++ reconstruction module is integrated into the VTK framework to allow for flexible analysis and visualization of the reconstructed image.

### 2.1 Reconstruction

Our reconstruction method relies on a splatting technique for high-quality interpolation, where each pixel of a B-mode images is smeared into a  $N \times M \times O$  kernel which is then either compounded or ‘alpha-blended’ into the 3D image reconstruction volume at the appropriate  $(x, y, z)$  location. The 2D B-mode images are splatted one-by-one as they are captured to provide real-time reconstruction.

Compounding requires the use of an accumulation buffer which is the same size (i.e. same number of voxels) as the reconstruction volume. For each pixel  $I_{\text{pixel}}$  in the B-mode images, the splat kernel coefficients  $b_k$  are calculated and then both the intensity values  $I_{k \text{ voxel}}$  for voxels in the reconstruction volume that are touched by the splat and the corresponding values  $a_k$  in the accumulation buffer are updated as follows:

$$I_{k \text{ voxel}} := (b_k I_{\text{pixel}} + a_k I_{k \text{ voxel}}) / (b_k + a_k) \quad (1)$$

$$a_k := b_k + a_k \quad (2)$$

Our second method, which we refer to as ‘alpha blending’ because it uses the same equation that is used for image compositing via alpha blending, provides interpolation without the use of an accumulation buffer:

$$I_{k \text{ voxel}} := b_k I_{\text{pixel}} + (1 - b_k) I_{k \text{ voxel}} \quad (3)$$

An additional heuristic is required here: the first time a voxel  $I_{k \text{ voxel}}$  is hit by a splat,  $I_{k \text{ voxel}} := I_{\text{pixel}}$ . Otherwise the initial voxel value of  $I_{k \text{ voxel}} = 0$  would be

blended into the final voxel value. In this method each new splat tends to obscure previous splats which hit the same voxels, whereas compounding provides an optimal averaging of the new splat with the previous splats.

In the case where the splat kernel is a single point  $a_0 = 1$ , these equations simplify respectively to those for pixel nearest neighbor (PNN) interpolation with compounding and PNN without compounding [7]. Of greater interest is a  $2 \times 2 \times 2$  kernel where  $a_k$  are trilinear interpolation coefficients, which corresponds to a splat that is a boxcar function with the same dimensions as a voxel of the reconstruction volume. We refer to reconstruction with this boxcar splat as pixel trilinear (PTL) interpolation, and apply it either with or without compounding. It provides higher quality reconstruction than PNN but is still fast enough to be used for real-time reconstruction.

In order to ensure that there are no gaps in the 3D image after reconstruction, the separation between B-mode ultrasound images must be less than the kernel width. This means a separation of less than 1 voxel width for PNN, and less than 2 voxel widths for PTL. In practice we found that maintaining a separation of approximately 1 voxel width (typically 0.5 mm) was not difficult to achieve after a short period of practice.

Note that the use of large kernels and radially symmetric splats with compounded reconstruction is equivalent to the radial basis function (RBF) [8] interpolation technique, which is very computationally intensive but produces very high quality reconstructions.

## 2.2 Data Flow Requirements for Real-Time Reconstruction

Among the significant problems associated with providing interactive visualization of the ultrasound volume during its reconstruction is the fact that the acquisition of tracking information from the POLARIS, the digitization of the ultrasound video stream, and the reconstruction of the 3D ultrasound volume all have to take place simultaneously in the background while the user interface for the application must continue to operate smoothly. We did not want the application interface to freeze while the reconstruction was taking place, but instead required that the user be able to adjust the view of the 3D ultrasound volume while the reconstruction progressed.

This interactivity is maintained by breaking the application into several threads that run in parallel, and by ensuring proper synchronization of data transfers between the threads. In total there are five threads that perform the following tasks (Fig. 1):

- (a) One thread waits for tracking information to arrive from the POLARIS via the serial port, converts the information to a  $4 \times 4$  matrix, and places the matrix onto a pre-allocated stack along with a timestamp. A spinlock (a “mutex lock” in modern programming terms) is used to ensure that both the tracking thread and the reconstruction thread can safely access the transformation stack without any possibility of data corruption.

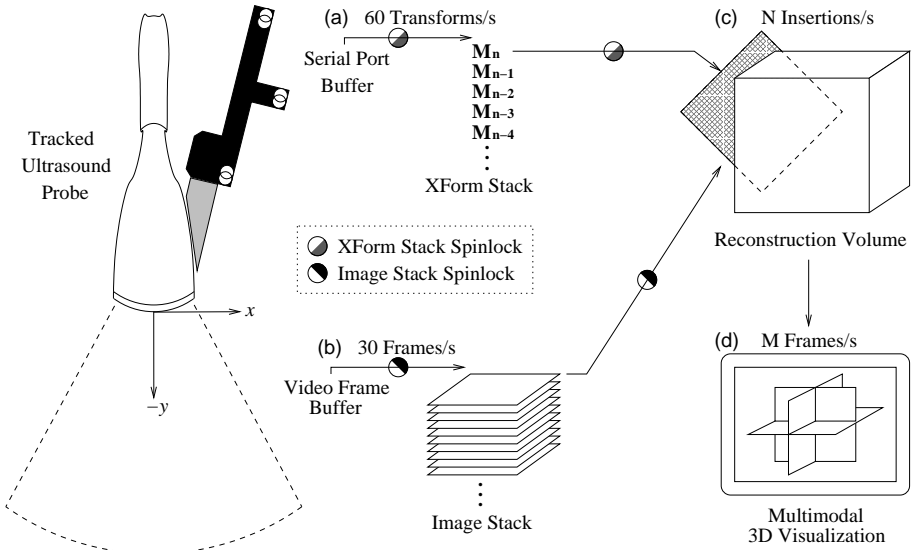


**Fig. 1.** Interactive 3D freehand ultrasound reconstruction/visualization.

- (b) A second thread moves each captured ultrasound video frame onto a stack along with a timestamp that describes when the video frame was digitized. Capture of the video at the full rate of 30 fps is guaranteed by the use of hardware interrupts and buffering within the video driver.
- (c) Two threads insert the most recent ultrasound video frame into the ultrasound reconstruction volume. Each of the two threads runs on one of the two processors in the computer: one thread performs the splats for the top half of the video frame and the other thread performs the splats for the bottom half. The rate  $N$  at which video frames can be inserted into the reconstruction volume depends on the available processor speed and on the interpolation method that is used. The position and orientation of the ultrasound probe for each video frame are interpolated from the stack of timestamped matrices from the tracking system, taking the lag of the video information relative to the tracking information into account.
- (d) The main application thread displays the partially reconstructed 3D ultrasound volume on the computer screen. The rate  $M$  at which the 3D view is refreshed is generally set to between 3 and 10 refreshes per second (lower than or equal to the rate  $N$  at which new video frames are inserted into the reconstruction volume).

Even if the reconstruction rate  $N$  is less than the 30 fps of the video feed, the video frames and the POLARIS tracking information are buffered at 30 fps and up to 60 measurements per second respectively. Once a freehand data-acquisition sweep has been completed, all of the video frames that were not previously used in the reconstruction can be compounded into the volume in order to further improve the final image quality.

### 2.3 Image Warping

Once the 3D ultrasound volume has been acquired, a manual nonlinear 3D registration can be performed to warp the 3D MRI to match the ultrasound volume. This registration is achieved via a 3D thin-plate spline, where the operator can drop a control point for the spline at any location in 3D space and, by then dragging the point to a new position with the mouse, interactively warp the MRI volume to match it to the ultrasound volume. We have previously reported on this technique [9,10] and will not cover it further here.

### 2.4 Validation with Deformable Phantoms

For validation of our methods, we have constructed a deformable PVA-cryogel [11] phantom that matches one of our 3D MRI anatomical data sets (see Fig. 2). The phantom is very soft, and we have enclosed it within a thermo-plastic shell that mimics the physical constraint provided by the cranium. A hole was left in the shell to provide access for an ultrasound probe. This phantom is suitable for imaging with MRI, CT or ultrasound.

The re-usable mould for the phantom was created via stereo laser lithography from a segmented MRI data set. The only significant difference between the mould and the cortical surface segmented from the data set is that the depths of some of the sulci were reduced before the mould was produced. This was necessary to ensure that the phantom could be removed from the mould after it was produced.

## 3 Results

Three slices through a reconstructed 3D ultrasound image are shown in Fig. 4. The reconstruction was done using our PTL compounded interpolation method from B-mode data cropped from video frames captured at  $320 \times 240$  resolution with 0.4 mm pixels. The reconstruction volume size was  $256 \times 193 \times 256$  and the voxel size was 0.4 mm. During the reconstruction, the display update rate for viewing the reconstructed volume (which is independent of the reconstruction rate) was limited to 5 updates per second due to the high computational load on the computer.

Magnified images of slices perpendicular to the original 2D B-mode scans are shown in Fig. 5 for each interpolation mode. The reconstructions were all done in real-time, and each image represents a different set of scan data. Because the POLARIS system provides a tracking accuracy of better than 0.4 mm (i.e. less than the voxel size) there are visible dislocation artifacts from jitter of the measured ultrasound probe position.

The noise in the images is noticeably reduced for PTL interpolated reconstruction relative to PNN reconstruction. The use of compounding also reduces the noise, but it must be noted that this effect depends on how slowly the operator moves the ultrasound probe during the scan. The use of compounding is

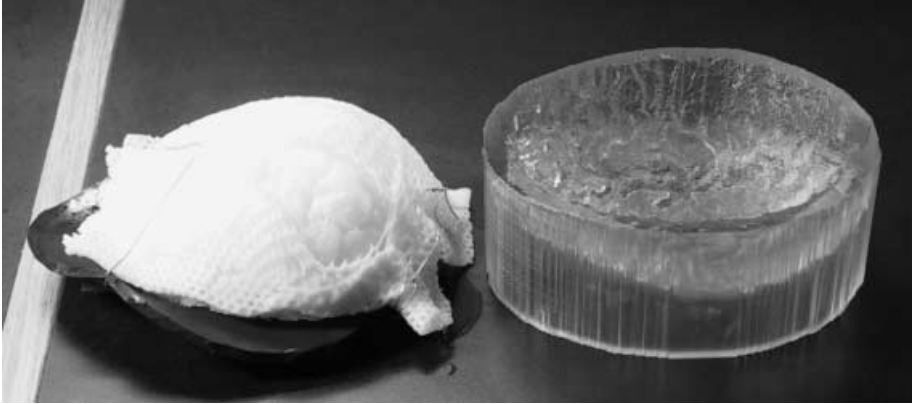


**Fig. 2.** The deformable PVA-cryogel phantom (left) and the mould (right) that was generated from a high-quality MRI scan of an actual brain.

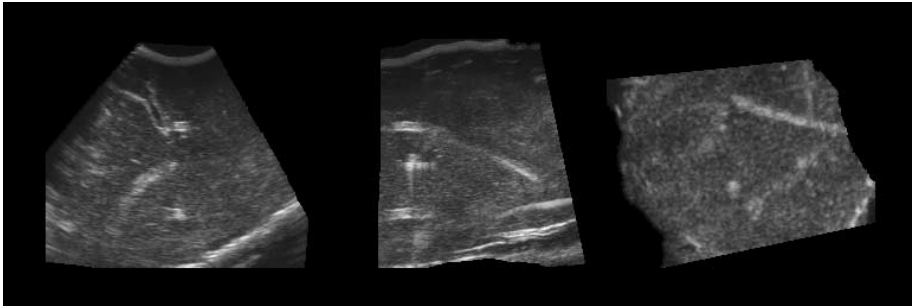


**Fig. 3.** Phantom image reconstructed by PTL via compounding, sliced in three orthogonal orientations. The maximum ultrasound scan depth was 8 cm, and one freehand scan sweep was performed to acquire the data. The phantom features that can be seen are the shallow ‘central sulcus’ that partially separates the two ‘hemispheres’ (upper left in first image) and thick strands of strongly echogenic PVA that are placed throughout the phantom (seen both lengthwise and in cross section).

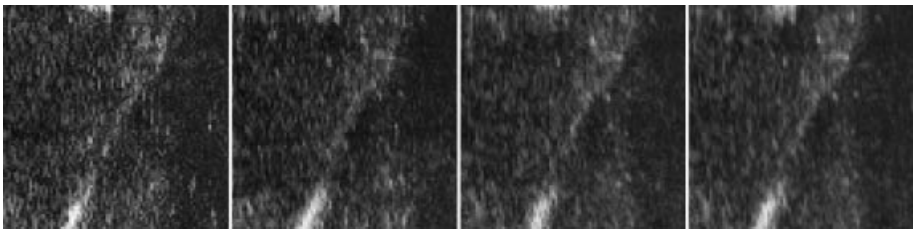


**Fig. 4.** From left to right: PNN, PNN with compounding, PTL via alpha blending, PTL via compounding. The noise in the image decreases as a result of both interpolation and compounding.

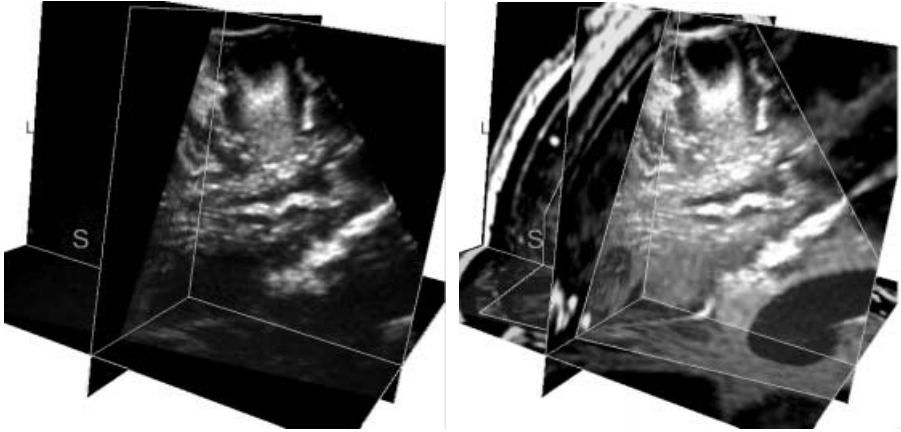


**Fig. 5.** A clinical 3D ultrasound image that we acquired through a craniotomy just prior to the removal of a small subdural tumor (seen at the top of the image). The image on the right includes an MRI image that has been linearly registered to the ultrasound image.

not expected to have any impact on quality unless the scan spacing is less than the voxel size, or unless the operator scans through the volume multiple times.

The reconstruction rate (i.e. the number of video frames splatted into the reconstruction volume per second) was the maximum possible value of  $30 \text{ s}^{-1}$  for the two PNN methods,  $20 \text{ s}^{-1}$  for PTL via alpha blending, and  $12 \text{ s}^{-1}$  for PTL via compounding. This is a very encouraging result, because  $30 \text{ s}^{-1}$  should be possible for all methods with a modern 2.2 GHz dual-CPU PC system.

We have used our system clinically for a transdural scan prior to a tumor excision. For this case the craniotomy was very small and no brain shift was noted. The image was captured and reconstructed within our in-house surgical guidance software package, and both the ultrasound and a pre-operative MRI were used for guidance during the surgical procedure.

## 4 Conclusion

We have demonstrated a technique for providing high-quality 3D freehand ultrasound reconstructions in real time on conventional PC hardware. This reconstruction technique is optimally suited for intra-operative use because the 3D image can be viewed before the scan is completed, and the operator can re-scan areas that were poorly covered on the first pass. The ultrasound volume can immediately be viewed as a multi-modal overlay on the pre-operative 3D MRI, and furthermore a manual nonlinear registration of the MRI to the ultrasound can be performed.

## Acknowledgments

The PVA-cryogel phantom used for this project was constructed by Kathleen Surry at The Robarts Research Institute. Our surgical navigation system was developed as a shared effort between the first author, Kirk Finnis, and Dr. Yves Starreveld of the London Health Sciences Centre. Dr. Starreveld also performed the intra-operative ultrasound scan, under the supervision of Dr. Wai Ng. Funding for this research is provided through grants from the Canadian Institutes for Health Research and the Institute for Robotics and Intelligent Systems.

## References

1. G. Unsgaard, S. Ommedal, T. Muller, A. Gronningsgaeter and T.A. Nagelhus Hernes. Neuronavigation by Intraoperative Three-dimensional Ultrasound: Initial Experience during Brain Tumor Resection. *Neurosurgery* **50**:804–812, 2002.
2. A. Gronningsgaeter, A. Kleven, S. Ommedal, T.E. Aerseth, T. Lie, F. Lindseth, T. Langø and G. Unsgård. SonoWand, an Ultrasound-based Neuronavigation System. *Neurosurgery* **47**:1373–1380, 2000.
3. D. L. G. Hill, C. R. Maurer Jr., R. J. Maciunas, J. A. Barwise, J. M. Fitzpatrick and M.Y. Wang. Measurement of Intraoperative Brain Surface Deformation under a Craniotomy. *Neurosurgery* **43**:514–528, 1998.
4. D. W. Roberts, A. Hartov, F. E. Kennedy, M. I. Miga and K. D. Paulsen. Intraoperative Brain Shift and Deformation: A Quantitative Analysis of Cortical Displacement in 28 Cases. *Neurosurgery* **43**:749–760, 1998.
5. W. Schroeder, K. W. Martin and W. Lorensen. *The Visualization Toolkit*, 2nd Edition. Prentice Hall, Toronto, 1998.
6. D.G. Gobbi and T.M. Peters, Generalized 3D nonlinear transformations for medical imaging: An object-oriented implementation in VTK, *Computerized Medical Imaging and Graphics*, accepted for publication, 2001.
7. R. Rohling, A. Gee, and L. Berman. A Comparison of Freehand Three-dimensional Ultrasound Reconstruction Techniques. *Medical Image Analysis* **3**:339–359.
8. R. Rohling, A. Gee, L. Berman and G. Treece. Radial Basis Function Interpolation for Freehand 3D Ultrasound. *Information Processing in Medical Imaging - IMP'99*. A. Kuba, M. Sámal and A. Todd-Pokropek (eds) Lecture Notes in Computer Science **1613**:478–483, Springer-Verlag, Berlin, 1999.
9. D.G. Gobbi, B.K.H. Lee, and T.M. Peters. Correlation of pre-operative MRI and intra-operative 3D ultrasound to measure brain tissue shift. *Proceedings of SPIE* **4319**:264–271, 2001.
10. D.G. Gobbi, R.M. Comeau and T.M. Peters. Ultrasound/MRI Overlay With Image Warping for Neurosurgery. *Medical Image Computing and Computer Assisted Intervention - MICCAI 2000*. Scott L. Delp, Anthony M. DiGioia, Branislav Jaramaz (eds) Lecture Notes in Computer Science **1935**:106–113, Springer-Verlag, Berlin, 2000.
11. I. Mano, H. Goshima, M. Nambu and I. Masahiro. New Polyvinyl Alcohol Gel Material for MRI Phantoms. *Magnetic Resonance in Medicine* **3**: 921–926, 1986.